

Magnetization orientation-induced topological phase transitions in a Chern insulator

Rui-An Chang^{1*} and Ching-Ray Chang^{2,3†}

¹*Graduate Institute of Applied Physics, National Taiwan University, Taipei 10617, Taiwan*

²*Department of Physics, National Taiwan University, Taipei 10617, Taiwan*

³*Center for Theoretical Physics, National Taiwan University, Taipei 10617, Taiwan*

So far, the highly-discussed topological phase transitions in Chern insulators have mostly been induced by tuning an intrinsic material parameter such as the exchange coupling strength. But it is not a practical way to induce topological phase transitions in real applications. Here we show that the topological phase transitions can be induced by tuning the extrinsic degree of freedom, magnetization orientation, in a two-dimensional electron gas with Dresselhaus [001] spin-orbit coupling and an exchange coupling to a ferromagnetic overlayer. In an analytic way, we show that this system has a topologically trivial phase with in-plane magnetization but undergoes a topological phase transition when the magnetization is deviated from the in-plane direction. The analytic results are further confirmed by numerical nonequilibrium Green functions calculations. With the combination of this phase transition and spin-transfer torque, a novel transistor can be designed with this promising fusion of topology and spintronics.

I. INTRODUCTION

Chern insulators, also known as quantum anomalous Hall (QAH) insulators, have been intensively studied for their fruitful physics and promising applications in future technology [1–10]. QAH systems attract the attention of researchers because they possess the topologically non-trivial chiral edge states in the absence of external magnetic field, which is of vital importance to the development of next-generation electronic devices. QAH states in proximity to superconductors, the chiral topological superconductors [11–17], also attract great attention because of the realization of Majorana fermions [18]. The first model of a QAH system is constructed by F. D. M. Haldane in the honeycomb lattice in 1988 [1]. A magnetic topological insulator (TI) was theoretically predicted to be a possible QAH system [3] and was later experimentally confirmed in a magnetic TI thin film [4, 5].

Between the preceding two groundbreaking and highly-discussed theoretical works, a two-band model [6], named as QWZ model in the following context, was proposed by Qi, Wu, and Zhang for describing a QAH system in a magnetic semiconductor heterostructure with spin-orbit coupling (SOC) induced by spatial inversion asymmetry. A two-dimensional electron gas (2DEG) can be formed in this system. That is to say, QWZ model can be understood as a spin-orbit coupled 2DEG with exchange coupling to a ferromagnetic (FM) overlayer, as shown in Fig. 1(a). Even with the aforementioned physical corresponding, QWZ model has mostly been treated as half of the well-known Bernevig-Hughes-Zhang model [19] of a topological insulator with time reversal symmetry. However, we claim that there should still be some fruitful physics about this simple but elegant model, especially in the topological aspect.

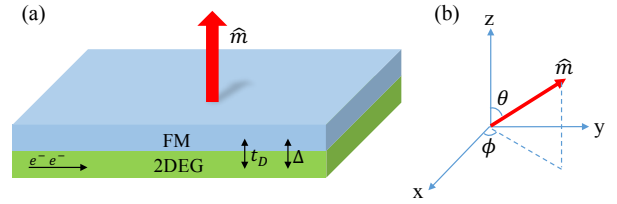


FIG. 1. (a) QWZ model is describing a spin-orbit coupled 2DEG with exchange coupling to an FM overlayer. Unlike the case in Ref. [6], the magnetization \hat{m} is a tunable degree of freedom in this work. t_D is the Dresselhaus [001] SOC and Δ is the exchange coupling. (b) θ is the polar angle and ϕ is the azimuthal angle. Generically \hat{m} can be in an arbitrary direction.

Until now, the topological phase transitions of QWZ model have been induced by tuning some material parameters such as the exchange coupling strength with the magnetization pointing to the z direction [6, 20, 21]. Nonetheless, the tuning of exchange coupling or any other material parameter is not easily realizable in practice because they are not allowed to be varied after the material was manufactured. Hence a more practical tunable degree of freedom should be chosen. Inspired by recent development of magnetization manipulation in spintronic research [22, 23], we anticipate that the topological phase transitions can be induced by tuning the magnetization orientation \hat{m} in QWZ model or any other similar 2DEG system, as shown in Fig. 1(b). In this conceptual framework, the magnetization orientation-induced topological phase transitions will be thoroughly investigated in a 2DEG with Dresselhaus [001] SOC and an exchange coupling to an FM overlayer. After the model and some background knowledge of topology are introduced, the topological phase diagrams will be obtained in an analytic way. Remarkably, an intuitive mathematical method is firmly employed to elucidate the interplay between magnetism and topology, instead of merely tak-

* r05245001@ntu.edu.tw

† crchang@phys.ntu.edu.tw

ing the numerical treatment. Furthermore, an idea of a novel transistor is presented according to our physical results. With the mature techniques of manufacturing 2DEG in a semiconductor heterostructure, the experimental realization of our theoretical prediction can be highly anticipated.

II. MODEL AND TOPOLOGICAL INVARIANT

According to QWZ model presented in the original paper [6], we can write down the Hamiltonian of this similar spin-orbit coupled 2DEG system with a tunable magnetization

$$H = \sum_{\mathbf{k}} \sum_{\alpha, \beta=\uparrow\downarrow} c_{\mathbf{k}\alpha}^\dagger H_{\alpha\beta}(\mathbf{k}) c_{\mathbf{k}\beta}, \quad (1)$$

where

$$H(\mathbf{k}) = -t_D \sin k_x \sigma_x + t_D \sin k_y \sigma_y + t(\cos k_x + \cos k_y) \sigma_z + \Delta \hat{m} \cdot \vec{\sigma}. \quad (2)$$

t_D is the strength of Dresselhaus [001] [24] SOC induced by inversion asymmetry, t is the kinetic hopping of an electron which would be set to be negative, and Δ is the exchange coupling. $c_{\mathbf{k}\alpha}^\dagger$ and $c_{\mathbf{k}\alpha}$ are creation and annihilation operators of an electron with momentum \mathbf{k} and spin α . Please note that the Zeeman term is $\Delta \hat{m} \cdot \vec{\sigma}$ but not $\Delta m_z \sigma_z$ that we usually meet in the literature because magnetization orientation \hat{m} has become a tunable degree of freedom in our discussion. The unit vector \hat{m} is $(\sin \theta \cos \phi, \sin \theta \sin \phi, \cos \theta)$ and $\vec{\sigma}$ is a three-dimensional vector whose components are Pauli matrices σ_x, σ_y , and σ_z . Before we start to investigate the topological property of this system, its real-space physical meaning can be appreciated by doing the Fourier transform of H into the real-space. In the real-space Hamiltonian

$$H = \sum_i c_{i+x}^\dagger \left(\frac{t}{2} \sigma_z - \frac{i}{2} t_D \sigma_x \right) c_i + c_{i+y}^\dagger \left(\frac{t}{2} \sigma_z + \frac{i}{2} t_D \sigma_y \right) c_i + h.c. + c_i^\dagger (\Delta \hat{m} \cdot \vec{\sigma}) c_i \quad (3)$$

where $c_i = (c_{i\uparrow} \ c_{i\downarrow})^T$, $c_{i\sigma}^\dagger$ and $c_{i\sigma}$ are creation and annihilation operators of an electron with spin $\sigma = \uparrow, \downarrow$ on the i^{th} site of a square lattice by which a 2DEG is mostly described. c_{i+x}^\dagger and c_{i+y}^\dagger stand for the hoppings of an electron in the x and y directions, respectively. The terms associated with t_D represent the Dresselhaus [001] SOC and the terms related to t and σ_z are understood as the effect of spin-dependent effective mass because different diagonal elements of σ_z indicate different kinetic hoppings ($\pm t$) for electrons with different spins. Therefore, the SOC and spin-dependent effective mass [6] appear in the real-space Hamiltonian along with the on-site Zeeman term with tunable magnetization orientation. With this real-space Hamiltonian, we can do the band structure calculations by doing the Fourier transform toward

the direction with periodic boundary condition. We will show the calculation results in the next section.

After the introduction of $H(\mathbf{k})$ and the appreciation of its real-space physical meaning, we can investigate the topological property of this system by calculating the topological invariant-Chern number. From the fact that a two-by-two Hermitian matrix can be written in the form of $\mathbf{d}(\mathbf{k}) \cdot \vec{\sigma}$, the x, y , and z components of vector $\mathbf{d}(\mathbf{k})$ are

$$\begin{aligned} d_x &= -t_D \sin k_x + \Delta \sin \theta \cos \phi, \\ d_y &= t_D \sin k_y + \Delta \sin \theta \sin \phi, \\ d_z &= t(\cos k_x + \cos k_y) + \Delta \cos \theta. \end{aligned} \quad (4)$$

For a generic model whose Hamiltonian has the form of $\mathbf{d}(\mathbf{k}) \cdot \vec{\sigma}$, we have the (first) Chern number [25]

$$C = \frac{1}{4\pi} \int_{BZ} dk_x dk_y \hat{\mathbf{d}} \cdot \left(\frac{\partial \hat{\mathbf{d}}}{\partial k_x} \times \frac{\partial \hat{\mathbf{d}}}{\partial k_y} \right), \quad (5)$$

where $\hat{\mathbf{d}}(\mathbf{k})$ is the unit vector of $\mathbf{d}(\mathbf{k})$ in \mathbf{d} -space. This integration is defined in the first Brillouin zone (BZ) with k_x and k_y ranging from $-\pi$ to π . In addition, if the system is half filled, the quantized Hall conductivity can be expressed through the Chern number [25, 26]

$$\sigma_{xy} = \frac{e^2}{h} C, \quad (6)$$

where e is the charge of an electron and h is the Planck constant. The expression in Eq. (5) has a direct geometrical interpretation and $\hat{\mathbf{d}}(\mathbf{k})$ totally determines the topological property of this system. The function $\hat{\mathbf{d}}(\mathbf{k})$ represents a mapping from the momentum space (BZ) to the sphere S^2 in \mathbf{d} -space, as shown in Fig. 2. This mapping can be denoted as $\hat{\mathbf{d}}(\mathbf{k}) : T^2 \rightarrow S^2$, where BZ $\in T^2$ (torus) in topology [20]. $(\frac{\partial \hat{\mathbf{d}}}{\partial k_x} \times \frac{\partial \hat{\mathbf{d}}}{\partial k_y})$ in the integrand of Eq. (5) is nothing but the Jacobian of the mapping from BZ to \mathbf{d} -space. $\hat{\mathbf{d}} \cdot (\frac{\partial \hat{\mathbf{d}}}{\partial k_x} \times \frac{\partial \hat{\mathbf{d}}}{\partial k_y})$ along with $dk_x dk_y$ is therefore an infinitesimal solid angle in \mathbf{d} -space mapped from an infinitesimal area $dk_x dk_y$ in the momentum space (BZ). From this geometrical interpretation, we can know that the integration divided by 4π is exactly how many times the vector $\hat{\mathbf{d}}(\mathbf{k})$ can wind around the origin as k_x and k_y run through the whole BZ. Therefore, the Chern number, an integration in two-dimensional BZ, is just the winding number of the vector $\hat{\mathbf{d}}(\mathbf{k})$ in three-dimensional \mathbf{d} -space. The geometrical analysis of the Chern number expression is not superfluous but important for appreciating the topological property of this system. As we will see, the topological phase transitions can be identified by the evolution of the sphere S^2 with respect to a certain degree of freedom such as θ .

In the next section, we will discuss how the vector $\mathbf{d}(\mathbf{k})$ behaves as k_x and k_y run through the whole BZ. The topological property of this system depends on if the \mathbf{d} -space origin is enclosed in the sphere S^2 traced out by the sweep of the vector $\mathbf{d}(\mathbf{k})$. This system is topologically nontrivial or trivial if the origin is or is not

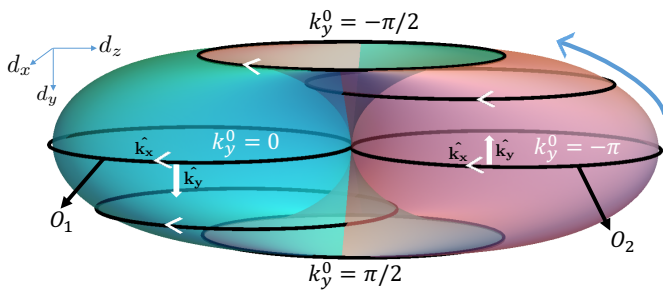


FIG. 2. Sphere S^2 formed by the sweep of $\mathbf{d}(\mathbf{k})$. Starting from the ellipse O_2 at $k_y^0 = -\pi$, many ellipses of Eq. (8) can be sequentially traced out along the direction of the curved arrowhead. Viewed from the $-d_y$ direction, the parameter k_x is evolving clockwise on each ellipse at each given value of $k_y = k_y^0$. Besides, k_y is evolving to the $+d_y$ direction when it is within $[-\pi/2, \pi/2]$; otherwise, k_y is evolving to the $-d_y$ direction. With the identification of the $\hat{\mathbf{k}}_x$ and $\hat{\mathbf{k}}_y$ directions on S^2 , the normal vector is defined by $\hat{\mathbf{k}}_x \times \hat{\mathbf{k}}_y$ (pointing to the outer side of S^2).

enclosed. Consequently, a very significant part of our work is to identify the critical state between the trivial and nontrivial phases, where the \mathbf{d} -space origin is on the boundary of the sphere S^2 .

III. TOPOLOGICAL PHASE TRANSITIONS

For the simplification of the following calculation, we assume ϕ to be zero such that \hat{m} lies on the $x-z$ plane. So the Eq. (4) becomes

$$\begin{aligned} d_x &= -t_D \sin k_x + \Delta \sin \theta, \\ d_y &= t_D \sin k_y, \\ d_z &= t(\cos k_x + \cos k_y) + \Delta \cos \theta. \end{aligned} \quad (7)$$

Now we are discussing how the sphere S^2 would be formed by the sweep of $\mathbf{d}(\mathbf{k})$ as k_x and k_y run through the whole BZ [Fig. 3(a)]. For a specific value of $k_y = k_y^0 \in [-\pi, \pi]$, an elliptical trajectory in \mathbf{d} -space is traced out on the plane of $d_y = t_D \sin k_y^0$ with k_x varying as a parameter from $-\pi$ to π . The equation of an ellipse corresponding to a value of $k_y = k_y^0$ is

$$\frac{(d_z - \Delta \cos \theta - t \cos k_y^0)^2}{t^2} + \frac{(d_x - \Delta \sin \theta)^2}{t_D^2} = 1 \quad (8)$$

, which is on the plane of $d_y = t_D \sin k_y^0$. Other ellipses can be formed under other specific values of k_y^0 , as shown in Fig. 2. After every point in the BZ is gone through, a collection of ellipses would be formed with their centers located on the ellipse

$$\begin{cases} d_y = t_D \sin k_y^0 \\ d_z = \Delta \cos \theta + t \cos k_y^0 \end{cases} \quad (9)$$

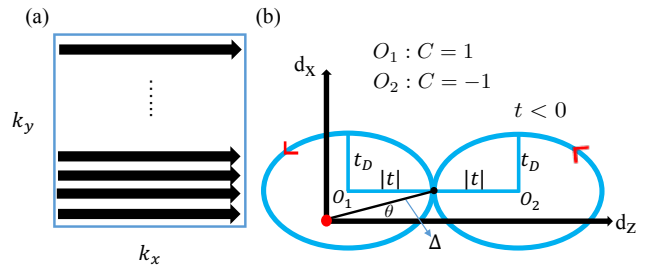


FIG. 3. (a) It shows how every point in the BZ is gone through. For a specific value of $k_y = k_y^0$, the line segment $k_x \in [-\pi, \pi]$ in the BZ maps to a closed elliptical trajectory in \mathbf{d} space as Eq. (8). (b) These two tangent ellipses correspond to $k_y^0 = -\pi, 0$. Actually, they are just O_2 and O_1 in Fig. 2 viewed from the $+d_y$ -direction. The topological property of this system is determined by the position of the origin (red dot) relative to these two ellipses: $C = 1$ or -1 if the origin is in O_1 or O_2 . (Note: (b) is not drawn according to the ratios of parameters.)

, which is on the plane of $d_x = \Delta \sin \theta$. In summary, S^2 is a collection of ellipses of Eq. (8) whose centers also form an ellipse. In Eq. (9), it is readily to see that the vector $\mathbf{d}(\mathbf{k})$ can only wrap the origin one time as we go through the whole BZ. Therefore, the Chern number C in Eq. (5) can only be 1, 0, or -1 .

Because of ϕ being set to zero, S^2 can only be shifted normally to d_y -direction when the magnetization is being tuned. That is to say, one just has to focus on the intersection of S^2 with the $d_y = 0$ plane and observe if the origin is enclosed in S^2 . The intersection is two ellipses corresponding to $k_y^0 = -\pi, 0$ ($d_y = 0$) in Eq. (8):

$$\frac{(d_z - \Delta \cos \theta \pm t)^2}{t^2} + \frac{(d_x - \Delta \sin \theta)^2}{t_D^2} = 1. \quad (10)$$

Actually, they are just O_2 and O_1 in Fig. 2, whose centers are $(\Delta \cos \theta - t, \Delta \sin \theta)$ and $(\Delta \cos \theta + t, \Delta \sin \theta)$ on the d_z - d_x plane, respectively, as shown in Fig. 3(b). If the origin is in O_1 or O_2 , the Chern number C is equal to 1 or -1 because an infinite line from the origin in O_1 to the negative z direction or that from the origin in O_2 to the positive z direction will inevitably pierce the inner or the outer surface of S^2 , respectively; otherwise, C is just zero when the origin is not enclosed [21] (the definition of surface orientation is presented in the caption of Fig. 2).

In the following, the mathematical requirements of topological phase transitions will be derived in order to obtain the phase diagrams. For the case of the origin in O_1 of Fig. 3(b), we have

$$\frac{(\Delta \cos \theta - |t|)^2}{t^2} + \frac{(\Delta \sin \theta)^2}{t_D^2} \leq 1, \quad 0 < \theta < \frac{\pi}{2}. \quad (11)$$

For the case of the origin in O_2 of Fig. 3(b), we have

$$\frac{(\Delta \cos \theta + |t|)^2}{t^2} + \frac{(\Delta \sin \theta)^2}{t_D^2} \leq 1, \quad \frac{\pi}{2} < \theta < \pi. \quad (12)$$

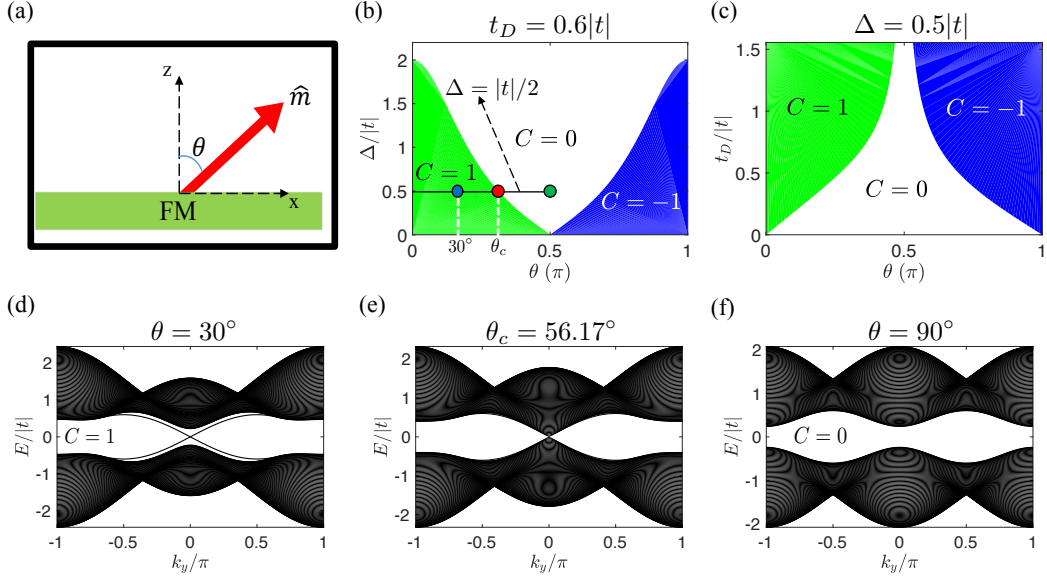


FIG. 4. Phase diagrams and energy bands. Topological phase transitions can be induced by the tuning of magnetization orientation $\hat{m} = (\sin \theta, 0, \cos \theta)$ in (a). In this figure, t is set to be -0.5 eV and other quantities are represented as units of $|t|$. (b) and (c) are phase diagrams of $\Delta - \theta$ and $t_D - \theta$ where the alternations of Chern number show the topological phase transitions in terms of θ (the tuning of \hat{m}). In (b) and (c), the green and blue regions represent topologically nontrivial phases where $C = 1$ and $C = -1$, respectively. The white regions ($C = 0$) stand for the topologically trivial phases. (d), (e), and (f) are energy bands of a strip which has an open boundary condition in the x -direction but a periodic boundary condition in the y -direction and respectively correspond to three representative values of θ in (b) under the case that $\Delta = |t|/2$ and $t_D = 0.6|t|$ (blue, red, and green dots on the black solid line). In the case of $\theta = 30^\circ$ (blue dot), chiral edge states are shown in (d) because of the topologically nontrivial phase with $C = 1$. In the case of $\theta = \theta_c = 56.17^\circ$ (red dot), (e) corresponds to a topological phase transition because the conduction band and valence band contact with each other. (f) is nothing but a topologically trivial phase (normal insulator) with $\theta = 90^\circ$ (green dot).

We expect to obtain the relation between t_D and θ . After doing some algebra we can get

$$t_D \geq \frac{\Delta |t| \sin \theta}{\sqrt{\Delta \cos \theta (2|t| - \Delta \cos \theta)}}, \quad 0 < \theta < \frac{\pi}{2} \quad (13)$$

for the origin in O_1 ($C = 1$) and

$$t_D \geq \frac{\Delta |t| \sin \theta}{\sqrt{-\Delta \cos \theta (2|t| + \Delta \cos \theta)}}, \quad \frac{\pi}{2} < \theta < \pi \quad (14)$$

for the origin in O_2 ($C = -1$). Please note that $2|t|$ needs to be larger than $\Delta |\cos \theta|$ inside the square roots of Eq. (13) and (14). Indeed, the requirement that $2|t| > \Delta |\cos \theta|$ is necessary to be satisfied or the origin is impossible to be enclosed in O_1 or O_2 in Fig. 3(b). From Eq. (13) and (14), we can respectively obtain the green ($C = 1$) and blue ($C = -1$) regions of the phase diagram that shows the relation between t_D and θ , as shown in Fig. 4(c). Topological phase transitions can be induced by the tuning of magnetization orientation at a certain value of t_D . In this case, the origin can be made to move into or out of the sphere S^2 as shown in Fig. 3(b). This is the topological mechanism to explain why the topological phase transition can be induced by tuning the magnetization orientation. Following the same procedure, the

relation between Δ and θ can also be obtained starting from Eq. (11) and (12):

$$\Delta \leq \frac{2t_D^2 |t| \cos \theta}{t_D^2 \cos^2 \theta + t^2 \sin^2 \theta}, \quad 0 < \theta < \frac{\pi}{2} \quad (15)$$

for the origin in O_1 ($C = 1$) and

$$\Delta \leq \frac{-2t_D^2 |t| \cos \theta}{t_D^2 \cos^2 \theta + t^2 \sin^2 \theta}, \quad \frac{\pi}{2} < \theta < \pi \quad (16)$$

for the origin in O_2 ($C = -1$). The phase diagram Fig. 4(b) can also be obtained according to Eq. (15) and (16) which correspond to the green region ($C = 1$) and the blue region ($C = -1$), respectively. The process of the topological phase transition induced by the magnetization orientation tuning is clearly presented from (d) to (f) in Fig. 4, corresponding to the origin moving out of the sphere S^2 as shown in Fig. 3(b). One thing should be emphasized is that, in Fig. 4(d) with $C = 1$, the number of chiral edge states on a strip with two edges along the y -direction is the double of $|C|$. It means that there is $|C|$ chiral edge state on each edge. This result conforms to the well-known bulk-edge correspondence [27], verifying the reliability of our band structure calculation and the analysis of the topological property.

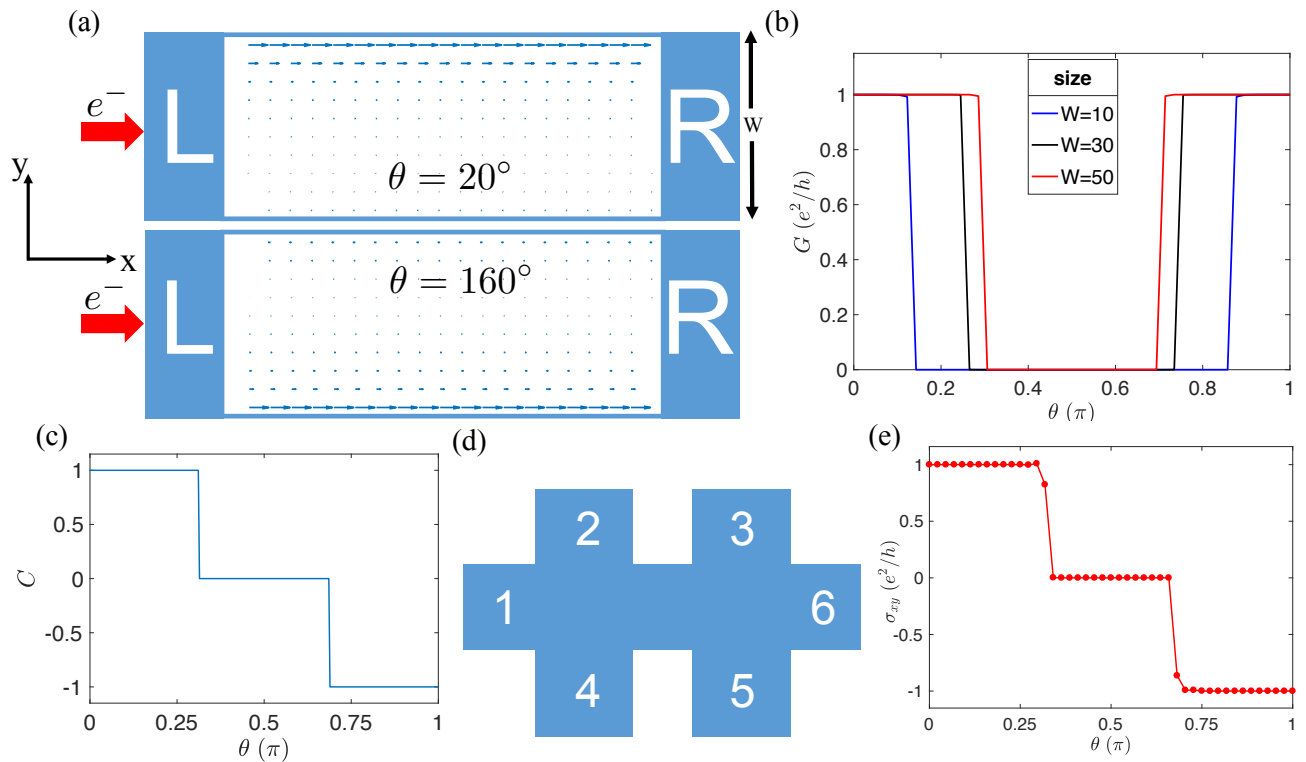


FIG. 5. NEGF calculation results. This set of figures show some numerical results confirming the analytic results mentioned in the previous section. In our calculations, parameters are set to be: $t = -0.5$ eV, $\Delta = |t|/2$, and $t_D = 0.6|t|$, the same as the setting of the black solid line in Fig. 4(b). In (a), the cases of $\theta = 20^\circ$ and $\theta = 160^\circ$ show opposite chirality, matching the fact that they possess different Chern numbers as shown in Fig. 4(b). In (b), the case with $W = 50$ demonstrates almost the same phase transition points approximately at $\theta = 0.31\pi$ and 0.69π as the Chern number in (c) extracted from Fig. 4(b). (d) is a six-terminal Hall-bar setup in which we can calculate the σ_{xy} . (e) is the relation between σ_{xy} and θ . It matches the Chern number in (c).

IV. NUMERICAL RESULTS

In the previous section, we successfully obtained the phase diagrams which show the topological phase transitions with respect to the magnetization orientation θ . The band structure calculations also clearly demonstrate the topological phase transition as predicted by our analytic results. However, all the previous results don't include the consideration of a bias voltage which would be very crucial in experiments. In this section, therefore, we employ the numerical nonequilibrium Green functions (NEGF) to investigate the transport properties of our system in the linear-response regime [28]. In the Landauer setup, the sample (central region) is contacted by the left lead and right lead, as shown in Fig. 5(a). Both the sample and the leads are made up of the system having been in discussion. Therefore, this Landauer setup in our NEGF calculations is a just like the system used to do the band structure calculations in the previous section. But the only difference here is that we rotate our system by $\pi/2$ clockwise in order to match the conventions of conductance or resistance that we are going to discuss later.

In NEGF calculations, one can obtain the lesser Green function $G^<(E)$ by using this widely-known formula [29]:

$$G^<(E) = G^R(E)\Sigma^<(E)G^A(E), \quad (17)$$

where $G^R(E)$ is the retarded Green function, $G^A(E)$ is $[G^R(E)]^\dagger$, and $\Sigma^<(E)$ is the lesser self-energy. Numerical calculation of the lesser Green function is a very standard technique. One can see the Appendix for relevant information. After knowing the numerical result of $G^<(E)$, the physical observable can be obtained through the density matrix

$$\hat{\rho} = \frac{1}{2\pi i} \int_{E_F - \Delta E/2}^{E_F + \Delta E/2} G^<(E) dE, \quad (18)$$

where $E_F = -0.01|t|$ is the Fermi energy lying in the bulk gap and $\Delta E = 1 \times 10^{-3}|t|$ is the potential energy drop between two leads with applied bias. In Fig. 5(a), we calculate the real-space local charge current flowing from site \mathbf{m} to its nearest neighbor site \mathbf{m}' with the definition [30]

$$J_{\mathbf{m}\mathbf{m}'} = \frac{e}{i\hbar} [c_{\mathbf{m}'}^\dagger t_{\mathbf{m}'\mathbf{m}} c_{\mathbf{m}} - \text{H.c.}], \quad (19)$$

where $t_{\mathbf{m}'\mathbf{m}}$ is the 2×2 hopping matrix from \mathbf{m} to \mathbf{m}' that can be found in the real-space Hamiltonian (3). One can see that the systems with different magnetization orientations corresponding to different Chern numbers ± 1 can demonstrate opposite chirality. In addition, there exists an unbalance of charge currents between two opposite edges due to the quantum anomalous Hall effect that makes electrons move along the transverse direction.

In Fig. 5(b), we calculate the conductance as functions of magnetization orientation θ at different sizes of the sample W by this formula [28]

$$G = \frac{e^2}{h} \text{Tr}(\Gamma_L G^R \Gamma_R G^A), \quad (20)$$

where $\Gamma_{L,R}$ is the level-broadening of the left and right leads, and $\text{Tr}(\Gamma_L G^R \Gamma_R G^A)$ is the transmission probability from the left to the right leads. For the definition of level-broadening, one can see the Appendix. In this calculation, the Fermi energy lies in the band gap, so the contribution to the conductance completely comes from the chiral edge states. With the increasing of the sample size (diminishing of the size effect), the conductance G of the case with $W = 50$ as a function of θ shows the same behavior of topological phase transitions as the Chern number in Fig. 5(c) extracted from the phase diagram in Fig. 4(b). Therefore, the analytically-obtained phase diagram in the previous section is consistent with the calculation of conductance using NEGF. In addition, the transmission is equal to $|C|$, conforming to the bulk-boundary correspondence.

However, the preceding numerical results are obtained from the two-terminal setup, in which the Hall conductance or resistance can not be calculated. Therefore, we add four more leads contacted to the upper and lower edges of the original two-terminal setup, as shown in Fig. 5(d). In this Hall-bar geometry, the voltage drops in the longitudinal and transverse directions can be obtained from the Landauer-Büttiker formula [29]

$$I_i = \frac{e^2}{h} \sum_j (T_{ji} V_i - T_{ij} V_j), \quad (21)$$

where I_i is the current flowing from the i^{th} lead into the sample, V_i is the voltage on the i^{th} lead, and T_{ji} is the transmission from the i^{th} to the j^{th} leads. In our NEGF calculation, we can obtain the transmissions T_{ji} between any two arbitrary leads with a voltage applied between the first and sixth leads. Consequently, we can solve Eq. (21) to get the voltage on each lead. The longitudinal and transverse resistances are given by

$$\rho_{xx} = \frac{V_3 - V_2}{I}, \quad \rho_{yx} = \frac{V_3 - V_5}{I}, \quad (22)$$

where I is the current injected into the sample from the first lead. Substitute ρ_{xx} and ρ_{yx} into the resistance-to-conductance conversion relations given by

$$\sigma_{xx} = \frac{\rho_{xx}}{\rho_{xx}^2 + \rho_{yx}^2}, \quad \sigma_{xy} = \frac{\rho_{yx}}{\rho_{xx}^2 + \rho_{yx}^2}, \quad (23)$$

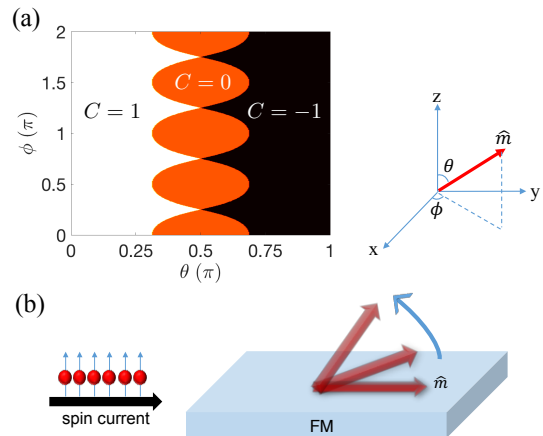


FIG. 6. (a) The setting of the parameters is $t = -0.5$ eV, $\Delta = |t|/2$, and $t_D = 0.6|t|$. This is the phase diagram in the case that θ and ϕ are both tunable degrees of freedom. The $C = 1$, 0, and -1 regions are characterized by white, red, and black, respectively. (b) When a spin current with z -polarization is injected into this system, the in-plane magnetization can be pulled up by STT, triggering the topological phase transition. Please note that \hat{m} is not necessary to be in the y -direction. This is only a schematic diagram.

we can successfully obtain the σ_{xy} whose plateau feature is very crucial in identifying the topologically nontrivial phases. Following the preceding procedure, we employ the NEGF to obtain the Hall conductance σ_{xy} as a function of magnetization orientation θ , as shown in Fig. 5(e). One can easily observe that the numerical result of σ_{xy} has a phase transition pattern nicely matching the Chern number in Fig. 5(c) which comes from the analytic result in the previous section. The proportionality between them conforms to Eq. (6). Therefore, we can also reach the consistency between the analytic results and transport calculations in the six-terminal Hall bar setup, as what we have done in the standard two-terminal case.

V. AZIMUTHAL DEGREE OF FREEDOM AND NOVEL TRANSISTOR

So far, we successfully grasp the phase transition behavior of our QAH system in discussion. But remember that the azimuthal angle ϕ of the magnetization orientation has been set to zero for convenience in analysis, as mentioned at the Sec. III. So we relax the degree of freedom ϕ and numerically calculate the Chern number given by Eq. (5). Fig. 6(a) is just the phase diagram showing the distribution of the Chern number with respect to θ and ϕ . In this phase diagram, topological phase transitions can be induced by tuning θ at an arbitrary value of ϕ , not only limited to the case with $\phi = 0$. The phase boundary (between $C = 1$ and 0 or $C = 0$ and -1) shows an oscillating behavior with respect to ϕ and its periodicity is $\pi/2$. More specifically, when ϕ is an odd multiple

of $\pi/4$, the topological phase transition happens between $C = \pm 1$, without $C = 0$. In another aspect, the topological phase transitions can also be induced by tuning ϕ at some specific values of θ , if θ is located within the left and right bounds of the red region ($C = 0$). That is to say, if we can somehow make the magnetization precess around the z -axis (*e.g.* microwave [31, 32]) with a proper θ and a constant angular velocity, the topological phase transitions can happen periodically. Such kind of time-dependent dynamics in the topological Floquet system [33, 34] is worth further investigation in the future, in which an effective electric field can be defined in \mathbf{k} -space [35]. From the fact that the integration of the effective magnetic field in \mathbf{k} -space (Berry curvature) is the Chern number, we can reasonably infer that an electric field analog is possibly related to topology as well.

With the understanding of the topological phase diagram (Fig. 6(a)), a novel transistor can be designed by the combination of topological phase transition and spin-transfer torque (STT) [22, 36]. Assume that this QAH system has an in-plane ($\theta = \pi/2$) magnetization at first. When a current with spin-polarization in the z -direction is injected into this system, the magnetization will experience an STT which can make it deviate from the in-plane direction, as shown in Fig. 6(b). According to the phase diagram, the resulting change of magnetization orientation is expected to induce a topological phase transition, but the phase transition point depends on the value of ϕ . Please note that the phase transition is allowable for the in-plane magnetization with an arbitrary value of ϕ . With the mature techniques of STT in the laboratories, such kind of STT-induced topological phase transition has a great potential being applied to topological spintronics. For example, the emergence of conducting chiral edge states in Figs. 4(d) or 5(a) can be controlled by the tuning of magnetization orientation through STT. Therefore, a conducting or insulating edge channel can respectively play the role of 1 or 0, and the tunable magnetization manipulated by STT is just similar to a valve. Of course, applying an external magnetic field can also manipulate the magnetization in which \hat{m} could be tuned to an arbitrary direction. However, this might not be as proper as STT for device manufacturing.

VI. SUMMARY AND OUTLOOK

Instead of tuning the intrinsic material parameters which are not practical in real applications, we successfully induce the topological phase transitions by tuning the magnetization orientation in a spin-orbit coupled 2DEG with an exchange coupling to an FM overlayer. The analytic results are confirmed by NEGF calculations with a small applied voltage, raising the possibility of experimental realization. At last, we present an idea of a novel transistor which may work with the combination of spin-transfer torque and topology, paving the way for low-dissipation electronic devices. Thanks to the ma-

ture techniques of manufacturing 2DEGs in semiconductor heterostructures, we expect our proposal to draw the attention from experimentalists.

In the future, the combination of Rashba and Dresselhaus SOCs in our system is worth further study, in which it will be interesting to investigate the interplay magnetization, topology, and persistent spin helix [37]. Beside 2DEG systems, magnetic topological insulators are also being studied intensively [38–41]. We can thereby apply the idea of tuning magnetization orientation to them. Therefore, a high Chern number system with tunable magnetization orientation is possible to be realized. More excitingly, the magnetization orientation can also be controlled in QAH systems placed in proximity to s -wave superconductors. The coupling between Majorana fermions and magnetism in chiral topological superconductors belonging to class D [42] may play a crucial role in topological quantum computations [43].

ACKNOWLEDGMENTS

This work is supported by the Ministry of Science and Technology of Taiwan under Grant No. MOST 107-2112-M-002-013-MY3.

Appendix: Nonequilibrium Green functions (NEGF)

This is a powerful tool to study the transport properties of electrons in nonequilibrium states, especially for a system applied with a small bias voltage. The essence of NEGF is to calculate the lesser Green function:

$$G^<(E) = G^R(E)\Sigma^<(E)G^A(E), \quad (\text{A.1})$$

where

$$G^R(E) = [E - H - \sum_p \Sigma_p(E - eV_p)]^{-1}. \quad (\text{A.2})$$

H is the Hamiltonian of Eq. (3), Σ_p and V_p are the self-energy and voltage of the lead p .

The lesser self-energy is

$$\Sigma^<(E) = i \sum_p \Gamma_p(E) f_p(E), \quad (\text{A.3})$$

where

$$\Gamma_p(E) = i[\Sigma_p(E - eV_p) - \Sigma_p^\dagger(E - eV_p)] \quad (\text{A.4})$$

and $f_p(E) = f_0(E - eV_p)$ are the level broadening and Fermi-Dirac distribution at zero-temperature of the lead p , respectively. Note that $eV_L - eV_R$ is simply the potential energy drop ΔE in the upper and lower limits of Eq. (18), where e is the charge of an electron, a negative quantity. For the calculation of level broadening, one can find the calculation techniques described in Ref. [28].

-
- [1] F. D. M. Haldane, *Phys. Rev. Lett.* **61**, 2015 (1988).
- [2] M. Z. Hasan and C. L. Kane, *Rev. Mod. Phys.* **82**, 3045 (2010).
- [3] R. Yu, W. Zhang, H.-J. Zhang, S.-C. Zhang, X. Dai, and Z. Fang, *Science* **329**, 61 (2010).
- [4] C.-Z. Chang, J. Zhang, X. Feng, J. Shen, Z. Zhang, M. Guo, K. Li, Y. Ou, P. Wei, L.-L. Wang, Z.-Q. Ji, Y. Feng, S. Ji, X. Chen, J. Jia, X. Dai, Z. Fang, S.-C. Zhang, K. He, Y. Wang, L. Lu, X.-C. Ma, and Q.-K. Xue, *Science* **340**, 167 (2013).
- [5] X. Kou, L. Pan, J. Wang, Y. Fan, E. S. Choi, W.-L. Lee, T. Nie, K. Murata, Q. Shao, S.-C. Zhang, and K. L. Wang, *Nat. Commun.* **6**, 8474 (2015).
- [6] X.-L. Qi, Y.-S. Wu, and S.-C. Zhang, *Phys. Rev. B* **74**, 085308 (2006).
- [7] J. Wang, B. Lian, H. Zhang, and S.-C. Zhang, *Phys. Rev. Lett.* **111**, 086803 (2013).
- [8] Y. Zhang and J. Shi, *Phys. Rev. Lett.* **113**, 016801 (2014).
- [9] J. Wu, J. Liu, and X.-J. Liu, *Phys. Rev. Lett.* **113**, 136403 (2014).
- [10] J. Wang, B. Lian, H. Zhang, Y. Xu, and S.-C. Zhang, *Phys. Rev. Lett.* **111**, 136801 (2013).
- [11] X.-L. Qi and S.-C. Zhang, *Rev. Mod. Phys.* **83**, 1057 (2011).
- [12] X.-L. Qi, T. L. Hughes, and S.-C. Zhang, *Phys. Rev. B* **82**, 184516 (2010).
- [13] C.-Z. Chen, Y.-M. Xie, J. Liu, P. A. Lee, and K. T. Law, *Phys. Rev. B* **97**, 104504 (2018).
- [14] C.-Z. Chen, J. J. He, D.-H. Xu, and K. T. Law, *Phys. Rev. B* **98**, 165439 (2018).
- [15] Y. Zeng, C. Lei, G. Chaudhary, and A. H. MacDonald, *Phys. Rev. B* **97**, 081102 (2018).
- [16] K. Sakurai, S. Ikegaya, and Y. Asano, *Phys. Rev. B* **96**, 224514 (2017).
- [17] Y.-T. Zhang, Z. Hou, X. C. Xie, and Q.-F. Sun, *Phys. Rev. B* **95**, 245433 (2017).
- [18] E. Majorana, *Nuovo Cimento* **14**, 171 (1937).
- [19] B. A. Bernevig, T. L. Hughes, and S.-C. Zhang, *Science* **314**, 1757 (2006).
- [20] C.-X. Liu, S.-C. Zhang, and X.-L. Qi, *Annu. Rev. Condens. Matter Phys.* **7**, 301 (2016).
- [21] J. K. Asbóth, L. Oroszlány, and A. Pályi, *A Short Course on Topological Insulators* (Springer, 2016).
- [22] F. Matsukura, Y. Tokura, and H. Ohno, *Nat. Nanotechnol.* **10**, 209 (2015).
- [23] J.-P. Hanke, F. Freimuth, C. Niu, S. Blügel, and Y. Mokrousov, *Nat. Commun.* **8**, 1479 (2017).
- [24] R. Winkler, *Spin-orbit Coupling Effects in Two-Dimensional Electron and Hole Systems* (Springer, 2003).
- [25] D. Xiao, M.-C. Chang, and Q. Niu, *Rev. Mod. Phys.* **82**, 1959 (2010).
- [26] D. J. Thouless, M. Kohmoto, M. P. Nightingale, and M. den Nijs, *Phys. Rev. Lett.* **49**, 405 (1982).
- [27] R. Jackiw and C. Rebbi, *Phys. Rev. D* **13**, 3398 (1976).
- [28] S. Datta, *Quantum Transport: Atom to Transistor* (Cambridge University Press, 2005).
- [29] S. Datta, *Electronic Transport in Mesoscopic Systems* (Cambridge University Press, 1997).
- [30] B. K. Nikolić, L. P. Zárbo, and S. Souma, *Phys. Rev. B* **73**, 075303 (2006).
- [31] F. Mahfouzi, N. Nagaosa, and B. K. Nikolić, *Phys. Rev. B* **90**, 115432 (2014).
- [32] F. Mahfouzi, B. K. Nikolić, S.-H. Chen, and C.-R. Chang, *Phys. Rev. B* **82**, 195440 (2010).
- [33] N. H. Lindner, G. Refael, and V. Galitski, *Nat. Phys.* **7**, 490 (2011).
- [34] L. DAlessio and M. Rigol, *Nat. Commun.* **6**, 8336 (2015).
- [35] S. Chaudhary, M. Endres, and G. Refael, *Phys. Rev. B* **98**, 064310 (2018).
- [36] J. Slonczewski, *Journal of Magnetism and Magnetic Materials* **159**, L1 (1996).
- [37] S.-H. Chen and C.-R. Chang, *Phys. Rev. B* **77**, 045324 (2008).
- [38] Y. Tserkovnyak and D. Loss, *Phys. Rev. Lett.* **108**, 187201 (2012).
- [39] A. N. Zarevad and J. Abouie, *Phys. Rev. B* **98**, 155413 (2018).
- [40] J. Wang, B. Lian, and S.-C. Zhang, *Phys. Rev. B* **93**, 045115 (2016).
- [41] M.-T. Tran, H.-S. Nguyen, and D.-A. Le, *Phys. Rev. B* **93**, 155160 (2016).
- [42] C.-K. Chiu, J. C. Y. Teo, A. P. Schnyder, and S. Ryu, *Rev. Mod. Phys.* **88**, 035005 (2016).
- [43] C. Nayak, S. H. Simon, A. Stern, M. Freedman, and S. Das Sarma, *Rev. Mod. Phys.* **80**, 1083 (2008).